Theory of the electron mobility in *n*-type 6H–SiC

T. Kinoshita[a] and K. M. Itoh[b]
Department of Applied Physics and Physico-Informatics, Keio University, Yokohama 223-8522, Japan

M. Schadt and G. Pensl
Institut für Angewandte Physik, Universität Erlangen-Nürnberg, D-91058 Erlangen, Germany

(Received 17 December 1998; accepted for publication 5 March 1999)

We report on calculations of the anisotropy of the electron Hall mobility and its temperature dependence in *n*-type 6H–SiC. The model is based on the conduction band structure determined recently by a first-principle calculation. It provides explicit and easy to use analytical expressions for both drift and Hall mobilities. The calculation of the Hall mobility based on our model agrees very well with experimentally determined anisotropic Hall mobility in 6H–SiC. © *1999 American Institute of Physics.* [S0021-8979(99)03512-4]

I. INTRODUCTION

Rapid progress of the SiC growth technology in the past decade has lead to a development of a wide variety of novel electronic devices having high operation temperatures, high breakdown voltages, low leakage currents, large thermal conductivities, and strong resistances against external radiation.[1] A large number of SiC devices are based on hexagonal polytypes, e.g., 4H and 6H–SiC, because of their peculiar material properties suited for the above-mentioned device applications.[2] One of the issues that needs to be addressed when fabricating electronic devices using hexagonal SiC is the fact that the electron mobility depends strongly on the crystallographic direction of traveling carriers due to the anisotropic structure of conduction bands. It was shown recently that the anisotropy of the electron Hall mobility in 6H–SiC could be as large as a factor of 4.5 at room temperature.[3] Quantitative understanding of such anisotropy is important especially for the designing of devices and development of reliable device simulators. Up to now both experimental[3,4] and computational[5–8] investigations on the anisotropy of the electron ''mobility'' have been performed on hexagonal SiC. The experimentalists have found a large anisotropy of the electron Hall mobility in 6H–SiC which depends on the crystallographic direction of the externally applied magnetic field and electronic current in Hall effect measurements.[3,4] In an effort to explain such large anisotropy, a number of Monte Carlo simulations of the electron drift mobility (NOT the Hall mobility!) has been performed and their results were compared directly to the experimental findings.[5–8] However, it is well known that the values of the drift mobility are different from those of the Hall mobility by a variable known as the Hall factor, i.e., a development of a theoretical model that allows for the calculation of the Hall mobility is needed for the direct comparison with experiments.[9]

In this work we present a theoretical model describing both the drift and Hall mobilities in 6H–SiC. The model is based on the conduction band structure determined recently by a first-principle calculation.[10,11] Unlike the results of the Monte Carlo simulation, our model provides explicit and easy to use analytical expressions for the drift and Hall mobilities. The mathematical model for the drift mobility may be useful for the device simulation while that for the Hall mobility allows for the direct comparison between theory and experiments. A numerical calculation of the Hall mobility as a function of temperature has been performed for the three distinct Hall measurement configurations shown in Fig. 1(a) [$\mathbf{j}\perp\mathbf{c},\mathbf{B}\parallel\mathbf{c}$], Fig. 1(b) [$\mathbf{j}\perp\mathbf{c},\mathbf{B}\perp\mathbf{c}$], and Fig. 1(c) [$\mathbf{j}\parallel\mathbf{c},\mathbf{B}\perp\mathbf{c}$], where $\mathbf{j}$ is the externally applied current vector, $\mathbf{B}$ is the magnetic field, and $\mathbf{c}$ is the direction of the *c* axis of a hexagonal unit cell. The result of our Hall mobility calculation for an *n*-type, nitrogen doped 6H–SiC single crystal is compared directly to the experimentally measured Hall mobilities in the three distinct Hall configurations.

II. METHOD AND MODEL

The band structure of 6H–SiC which we employed in this work is shown in Fig. 2. There are six semiellipsoidal constant energy surfaces for electrons centered exactly at *M* points in the first Brillouin zone. The conduction band structures along three principle axes, i.e., the directions along $M-\Gamma$, $M-K$, and $M-L$ points shown in Fig. 2, are assumed to be parabolic. The effective masses in $M-\Gamma$, $M-K$, and $M-L$ directions are $m_1^*=0.75m_0$, $m_2^*=0.24m_0$, and $m_3^*=1.83m_0$, respectively, where m_0 is the free electron rest mass. This band structure for 6H–SiC is a simplified version of the recent advanced first-principle calculation which predict six semidumbbell shaped constant energy surfaces centered exactly at *M* points, i.e., there are 12 equivalent conduction band minima at points between *M* and *L*.[10,11] The dumbbells are replaced with ellipsoids here since the center dips in the dumbbells at *M* points predicted by theory are reasonably small (~10 meV) and they can be neglected for our kind of low-field mobility study. The values of m_1^*, m_2^*, and m_3^* listed above have been estimated from the parabolic

[a]Present address: Hitachi Research Laboratory, Hitachi 319-1292, Japan.
[b]Electronic mail: kitoh@appi.keio.ac.jp

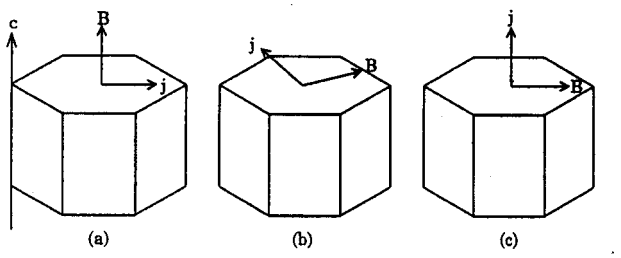

FIG. 1. Schematic diagram of the three distinct Hall measurement configurations: (a) [$\mathbf{j}\perp\mathbf{c},\mathbf{B}\|\mathbf{c}$], (b) [$\mathbf{j}\perp\mathbf{c},\mathbf{B}\perp\mathbf{c}$], and (c) [$\mathbf{j}\|\mathbf{c},\mathbf{B}\perp\mathbf{c}$].

fitting of the curvature of the conduction band minimum given by theory,[10] and are in good agreement with experimentally found values of effective masses.[12]

Our strategy for obtaining the drift and Hall mobility consists of the following steps. First, we will derive an expression for the conductivity tensor including the magnetic field for one ellipsoid. We will then place three ellipsoids in proper positions in the reciprocal space and find the total conductivity tensor by adding the contribution from each of the three ellipsoids. This procedure will lead to analytical expressions for the drift and Hall mobilities as a function of the average electron relaxation time and the effective masses. Calculation of the average relaxation time will be presented at the end.

The electronic current vector $\mathbf{J}'$ for one ellipsoid in the presence of the magnetic field is given by[13]

$$\mathbf{J}'=\boldsymbol{\sigma}'\mathbf{E}'=\begin{pmatrix}\sigma'_{11} & -\sigma'_{12}B'_3 & \sigma'_{13}B'_2\\ \sigma'_{21}B'_3 & \sigma'_{22} & -\sigma'_{23}B'_1\\ -\sigma'_{31}B'_2 & \sigma'_{32}B'_1 & \sigma'_{33}\end{pmatrix}\mathbf{E}', \quad (1)$$

where the components of the conductivity tensor σ' are given by

$$\sigma'_{ii}=\frac{q^2}{k_BT}\sum_{\mathbf{k}}\tau_{\mathbf{k}}f_0(\epsilon)v_i^2, \quad (2a)$$

$$\sigma'_{ij}=\frac{q^3}{m_j^*k_BT}\sum_{\mathbf{k}}\tau_{\mathbf{k}}f_0(\epsilon)v_i^2, \quad (2b)$$

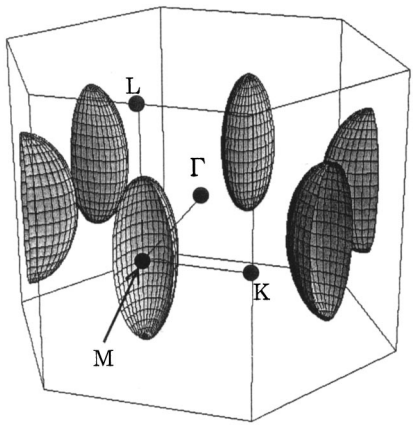

FIG. 2. Scheme of the 6H–SiC Brillouin zone used in this study; six semiellipsoids are contained in the hexagonal first Brillouin zone.

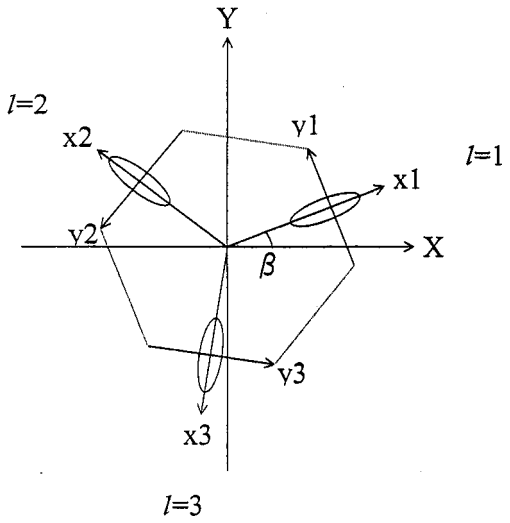

FIG. 3. Top view of the Brillouin zone revealed in Fig. 2 showing configurations of the ellipsoids and the coordinate axes used for the derivation of Eq. (9).

$\mathbf{E}'$ is the applied electric field vector, q is the electron charge, T is the temperature, $\tau_{\mathbf{k}}$ is the relaxation time for an electron having wave vector $\mathbf{k}$, $f_0(\epsilon)\approx\exp[-(\epsilon-\epsilon_F)/k_BT]$ is the Fermi function for an electron of energy ϵ, $B'_{i=1,2,3}$ is the i component of magnetic field, $m^*_{j=1,2,3}$ is the j component of the effective mass, and $v_{k=1,2,3}$ is the k component of the electron velocity. The subscripts $i,j,k=1,2,3$ correspond to the x, y, and z directions for one ellipsoid taken along the $M-\Gamma$, $M-K$, and $M-L$ direction, respectively. Each component of $\mathbf{k}$ and $\mathbf{v}$ in a spherical coordinate system is given by;

$$k_1=\frac{\sqrt{2m_1^*\epsilon}}{\hbar}\cos\phi\sin\theta, \quad (3a)$$

$$k_2=\frac{\sqrt{2m_2^*\epsilon}}{\hbar}\sin\phi\sin\theta, \quad (3b)$$

$$k_3=\frac{\sqrt{2m_3^*\epsilon}}{\hbar}\cos\theta, \quad (3c)$$

$$h_1=\frac{m_1^*v_1^2}{2\epsilon}=\cos^2\phi\sin^2\theta, \quad (4a)$$

$$h_2=\frac{m_2^*v_2^2}{2\epsilon}=\sin^2\phi\sin^2\theta, \quad (4b)$$

$$h_3=\frac{m_3^*v_3^2}{2\epsilon}=\cos^2\theta. \quad (4c)$$

Inserting Eqs. (3a)–(3c) and Eqs. (4a)–(4c) in Eqs. (2a) and (2b), and by changing the variables

$$\sum_{\mathbf{k}}\simeq\frac{2}{(2\pi)^3}\int_{\mathbf{k}}d\mathbf{k}, \quad (5)$$

$$d\mathbf{k}=\frac{\sqrt{2m_1^*m_2^*m_3^*}}{\hbar^3}k_BT\sqrt{k_BTx}\sin\theta\,d\theta\,d\phi\,dx,$$

where

$$x=\frac{\epsilon}{k_BT}, \tag{6}$$

we obtain

$$\sigma'_{ii}=qn'\frac{q}{m_i^*}\frac{4}{3\sqrt{\pi}}\frac{3}{4\pi}\int_0^\infty\int_0^{2\pi}\int_0^{\pi}\tau_{\mathbf{k}}x^{3/2}h_ie^{-x}$$

$$\times\sin\theta\,d\theta\,d\phi\,dx=qn'\frac{q}{m_i^*}\langle\tau_{\mathbf{k}}\rangle_i, \tag{7a}$$

$$\sigma'_{ij}=qn'\frac{q^2}{m_i^*m_j^*}\frac{4}{3\sqrt{\pi}}\frac{3}{4\pi}\int_0^\infty\int_0^{2\pi}\int_0^{\pi}\tau_{\mathbf{k}}^2x^{3/2}h_ie^{-x}$$

$$\times\sin\theta\,d\theta\,d\phi\,dx=qn'\frac{q^2}{m_i^*m_j^*}\langle\tau_{\mathbf{k}}^2\rangle_i, \tag{7b}$$

where n' is the electron concentration in each ellipsoid given by

$$n'=2\left(\frac{m^*k_BT}{2\pi\hbar^2}\right)^{3/2}e^{-(E_C-E_F)/k_BT}, \tag{8}$$

where E_C and E_F are the energy of the conduction band and Fermi level, respectively. The total electron concentration n is given by a relation $3n'=n$.

Now we place three ellipsoids labeled $l=1,2,3$ in the k space as shown in Fig. 3. Figure 3 is the top view of Fig. 2 with all the six semiellipsoids combined into three full ellipsoids. So far $\mathbf{J}'_{l=1}$, $\mathbf{J}'_{l=2}$, and $\mathbf{J}'_{l=3}$ of Eq. (1) is written for the independent coordinate systems $x_1-y_1-z_1$, $x_2-y_2-z_2$, and $x_3-y_3-z_3$, respectively. The following transformation leads to the expressions for $\mathbf{J}_{l=1,2,3}$ that are written for the $X-Y-Z$ coordinate system shown in Fig. 3

$$\mathbf{J}_l=\begin{bmatrix}\cos\alpha_l & -\sin\alpha_l & 0\\ \sin\alpha_l & \cos\alpha_l & 0\\ 0 & 0 & 1\end{bmatrix}\mathbf{J}'_l, \tag{9}$$

where

$$\alpha_l=\beta+\frac{2\pi(l-1)}{3}. \tag{10}$$

Finally we obtain the total current $\mathbf{J}$ in the $X-Y-Z$ coordinate system as

$$\mathbf{J}=\sigma\mathbf{E}=\begin{bmatrix}\sigma_{11} & \sigma_{12} & \sigma_{13}\\ \sigma_{21} & \sigma_{22} & \sigma_{23}\\ \sigma_{31} & \sigma_{32} & \sigma_{33}\end{bmatrix}\mathbf{E},$$

$$=\sum_l\mathbf{J}_l$$

$$=\frac{3}{2}\begin{bmatrix}\sigma'_{11}+\sigma'_{22} & -(\sigma'_{12}+\sigma'_{12})B_3 & (\sigma'_{13}+\sigma'_{23})B_2\\ (\sigma'_{12}+\sigma'_{21})B_3 & \sigma'_{11}+\sigma'_{22} & -(\sigma'_{13}+\sigma'_{23})B_1\\ -(\sigma'_{31}+\sigma'_{32})B_2 & (\sigma'_{31}+\sigma'_{32})B_1 & 2\sigma'_{33}\end{bmatrix}\begin{bmatrix}E_1\\E_2\\E_3\end{bmatrix}, \tag{11}$$

where B_{1-3} and E_{1-3} are the components of $\mathbf{B}$ and $\mathbf{E}$ in the $X-Y-Z$ coordinate system. Thus the conductivity tensor σ in the $X-Y-Z$ coordinate system is given by

$$\sigma=\frac{3}{2}\begin{bmatrix}\sigma'_{11}+\sigma'_{22} & -(\sigma'_{12}+\sigma'_{21})B_3 & (\sigma'_{13}+\sigma'_{23})B_2\\ (\sigma'_{12}+\sigma'_{21})B_3 & \sigma'_{11}+\sigma'_{22} & -(\sigma'_{13}+\sigma'_{23})B_1\\ -(\sigma'_{31}+\sigma'_{32})B_2 & (\sigma'_{31}+\sigma'_{32})B_1 & 2\sigma'_{33}\end{bmatrix}. \tag{12}$$

The standard formula for σ in a semiconductor is given by:[14]

$$\sigma=3n'q\begin{bmatrix}\mu_1 & 0 & 0\\ 0 & \mu_2 & 0\\ 0 & 0 & \mu_3\end{bmatrix}\begin{bmatrix}1 & -\mu_{H12}B_3 & \mu_{H13}B_2\\ \mu_{H21}B_3 & 1 & -\mu_{H23}B_1\\ -\mu_{H31}B_2 & \mu_{H32}B_1 & 1\end{bmatrix}, \tag{13}$$

where μ_{1-3} are the components of the drift mobility and $\mu_{H1-3,1-3}$ are the components of the Hall mobility. By comparing Eqs. (12) and (13), we obtain the following analytical expressions for the drift and Hall mobilities:

$$\mu_1=\mu_2=\frac{q}{2}\left(\frac{\langle\tau_{\mathbf{k}}\rangle_1}{m_1^*}+\frac{\langle\tau_{\mathbf{k}}\rangle_2}{m_2^*}\right), \tag{14a}$$

$$\mu_3=\frac{q\langle\tau_{\mathbf{k}}\rangle_3}{m_3^*}, \tag{14b}$$

$$\mu_{H12}=\mu_{H21}=q\frac{\langle\tau_{\mathbf{k}}^2\rangle_1+\langle\tau_{\mathbf{k}}^2\rangle_2}{m_1^*\langle\tau_{\mathbf{k}}\rangle_2+m_2^*\langle\tau_{\mathbf{k}}\rangle_1}, \tag{14c}$$

$$\mu_{H13}=q\frac{m_2^*\langle\tau_{\mathbf{k}}^2\rangle_1+m_1^*\langle\tau_{\mathbf{k}}^2\rangle_2}{m_1^*m_3^*\langle\tau_{\mathbf{k}}\rangle_2+m_2^*m_3^*\langle\tau_{\mathbf{k}}\rangle_1}, \tag{14d}$$

$$\mu_{H31}=\frac{q}{2}\left(\frac{\langle\tau_{\mathbf{k}}^2\rangle_3}{m_1^*\langle\tau_{\mathbf{k}}\rangle_3}+\frac{\langle\tau_{\mathbf{k}}^2\rangle_3}{m_2^*\langle\tau_{\mathbf{k}}\rangle_3}\right). \tag{14e}$$

Equations (14a)–(14e) allow to calculate the drift and Hall mobility for arbitrary crystallographic directions if the values of $\langle\tau_{\mathbf{k}}\rangle_{1-3}$ and $\langle\tau_{\mathbf{k}}^2\rangle_{1-3}$ are known. For the three Hall measurement configurations (a) $[\mathbf{j}\perp\mathbf{c},\mathbf{B}\parallel\mathbf{c}]$, (b) $[\mathbf{j}\perp\mathbf{c},\mathbf{B}\perp\mathbf{c}]$, and (c) $[\mathbf{j}\parallel\mathbf{c},\mathbf{B}\perp\mathbf{c}]$ shown in Fig. 1, we find the following expressions for the Hall mobility $\mu_{H(\mathrm{a})}$, $\mu_{H(\mathrm{b})}$, and $\mu_{H(\mathrm{c})}$:

$$\mu_{H(\mathrm{a})}=\frac{\sigma'_{12}+\sigma'_{21}}{\sigma'_{11}+\sigma'_{22}}, \tag{15a}$$

$$\mu_{H(\mathrm{b})}=\frac{\sigma'_{31}+\sigma'_{32}}{\sigma'_{33}}, \tag{15b}$$

$$\mu_{H(\mathrm{c})}=\frac{\sigma'_{13}+\sigma'_{23}}{\sigma'_{11}+\sigma'_{22}}. \tag{15c}$$

In order to calculate the drift and Hall mobilities using Eqs. (14a)–(14e) and Eqs. (15a)–(15c), one needs to find $\langle\tau_{\mathbf{k}}\rangle_{1-3}$ and $\langle\tau_{\mathbf{k}}^2\rangle_{1-3}$ based on carrier scattering theory in semiconductors. For that purpose, we have considered four scattering mechanisms: ionized impurity scattering, acoustic phonon scattering, first order optical phonon scattering, and intervalley scattering. Among these four scattering mechanisms the ionized impurity scattering rate is the most sensitive with respect to the band structure anisotropy. Therefore, we have used the following expression, which takes into account the effect of anisotropy, for the calculation of the relaxation time τ_{ion} for ionized impurity scattering:

$$\frac{1}{\tau_{\mathrm{ion}}}=\frac{1}{(2\pi)^3}\frac{2\pi}{\hbar}\frac{\sqrt{2m_1^*m_2^*m_3^*}}{\hbar^3}\sqrt{\epsilon}\times\int_0^{2\pi}\int_0^{\pi}|\mathbf{H}_{\mathbf{k}'\mathbf{k}}|^2\frac{\mathbf{v}_{\mathbf{k}}(\mathbf{v}_{\mathbf{k}}-\mathbf{v}_{\mathbf{k}'})}{\mathbf{v}_{\mathbf{k}}^2}\sin\theta\,d\theta\,d\phi, \tag{16}$$

where $\mathbf{V}_{\mathbf{k}}$ and $\mathbf{V}_{\mathbf{k}'}$ are the velocity of incident and scattered electrons having wave vectors $\mathbf{k}$ and $\mathbf{k}'$, respectively. The matrix element $H_{\mathbf{k}\mathbf{k}'}$ is given by:[15]

$$H_{\mathbf{k}'\mathbf{k}}=-\frac{4\pi n_{\mathrm{ion}}q^2}{\kappa}\frac{1}{|\mathbf{k}-\mathbf{k}'|^2+L_D^{-2}}, \tag{17}$$

where n_{ion} is the concentration of the ionized impurity, κ is the dielectric constant, and L_D is the screening length given by

$$L_D=\left(\frac{\kappa k_BT}{4\pi q^2}\right)^{1/2}\left(n+\frac{(N_{MJ}-N_{MN}-n)(N_{MN}+n)}{N_{MJ}}\right)^{-1/2}, \tag{18}$$

where N_{MJ} and N_{MN} are the concentration of the majority and minority impurities, respectively. The scattering rate τ_{op}^{-1} for the first-order optical phonon scattering is given by:[16]

$$\frac{1}{\tau_{\mathrm{op}}}=\frac{(2m_{\mathrm{ds}}^*)^{5/2}D_{\mathrm{op}}^2}{\pi\rho k_B\Theta_{\mathrm{op}}\hbar^4}\left(\frac{(\epsilon+k_B\Theta_{\mathrm{op}})^{1/2}(2\epsilon+k_B\Theta_{\mathrm{op}})}{\exp(\Theta_{\mathrm{op}}/T)-1}+\frac{\mathrm{Re}(\epsilon-k_B\Theta_{\mathrm{op}})^{1/2}(2\epsilon-k_B\Theta_{\mathrm{op}})}{1-\exp(-\Theta_{\mathrm{op}}/T)}\right), \tag{19}$$

where m_{ds}^* is the density of the state effective mass given by $(m_1^*m_2^*m_3^*)^{1/3}$, D_{op} is the optical phonon deformation potential, and Θ_{op} is the optical phonon temperature. Acoustic phonon deformation scattering rate τ_{ac}^{-1} is given by:[17]

$$\tau_{\mathrm{ac}}^{-1}=\frac{\sqrt{2}(k_BTm_{\mathrm{ds}}^*)^{3/2}D_{\mathrm{ac}}^2}{\pi\hbar^4\rho v_s^2}x^{1/2}, \tag{20}$$

where D_{ac} is the acoustic phonon deformation potential, ρ is the density, and v_s is the sound velocity in the particular semiconductor. For intervalley scattering, we consider two processes involving phonons of temperatures Θ_2 and Θ_3. The scattering $\tau_{\mathrm{intv}}^{-1}$ is given by:[18]

$$\frac{1}{\tau_{\mathrm{intv}}}=\tau_{\mathrm{ac}}^{-1}\left[\sum_{i=2}^{3}\frac{w_i}{w_1}\left(\frac{\Theta_i}{T}\right)^{3/2}\left(\frac{(xT/\Theta_i+1)^{1/2}}{\exp(\Theta_i/T)-1}+\frac{\mathrm{Re}(xT/\Theta_i-1)^{1/2}}{1-\exp(-\Theta_i/T)}\right)\right], \tag{21}$$

where w_i/w_1 is the coupling constant. Finally, we obtain the average relaxation time by:

$$\langle\tau_{\mathbf{k}}\rangle_i=\frac{4}{3\sqrt{\pi}}\frac{3}{4\pi}\int_0^{\infty}\int_0^{2\pi}\int_0^{\pi}\frac{1}{\tau_{\mathrm{ion}}^{-1}+\tau_{\mathrm{op}}^{-1}+\tau_{\mathrm{ac}}^{-1}+\tau_{\mathrm{intv}}^{-1}}x^{3/2}h_ie^{-x}\times\sin\theta\,d\theta\,d\phi\,dx, \tag{22}$$

$$\langle\tau_{\mathbf{k}}^2\rangle_i=\frac{4}{3\sqrt{\pi}}\frac{3}{4\pi}\times\int_0^{\infty}\int_0^{2\pi}\int_0^{\pi}\left(\frac{1}{\tau_{\mathrm{ion}}^{-1}+\tau_{\mathrm{op}}^{-1}+\tau_{\mathrm{ac}}^{-1}+\tau_{\mathrm{intv}}^{-1}}\right)^2x^{3/2}h_ie^{-x}\times\sin\theta\,d\theta\,d\phi\,dx. \tag{23}$$

Values of τ's and h_i are given by Eqs. (16)–(21) and Eqs. (4a)–(4c), respectively. Calculation of the drift and Hall mobility is performed by inserting Eqs. (22) and (23) into Eqs. (14a)–(14e).

III. COMPARISON WITH EXPERIMENTS

We have performed Hall effect measurements on a nitrogen doped, *n*-type 6H–SiC sample in order to obtain Hall mobilities for the three configurations shown in Fig. 1. The concentration of nitrogen donors at hexagonal sites $N_h=1.15\times10^{16}\,\mathrm{cm}^{-3}$, of nitrogen in cubic sites $N_c=2.3\times10^{16}\,\mathrm{cm}^{-3}$, and of compensating acceptors $N_A=1.10\times10^{16}\,\mathrm{cm}^{-3}$ are found by fitting the cubic neutrality equation to the temperature dependence of n. Details of these experimental and fitting procedures are given in Ref. 3. Our purpose is to calculate the Hall mobilities for this particular 6H–SiC sample and to compare them with experimentally measured mobilities in the three configurations. Values of all the parameters needed for our 6H–SiC mobility calculation have been obtained in our previous theoretical work involv-

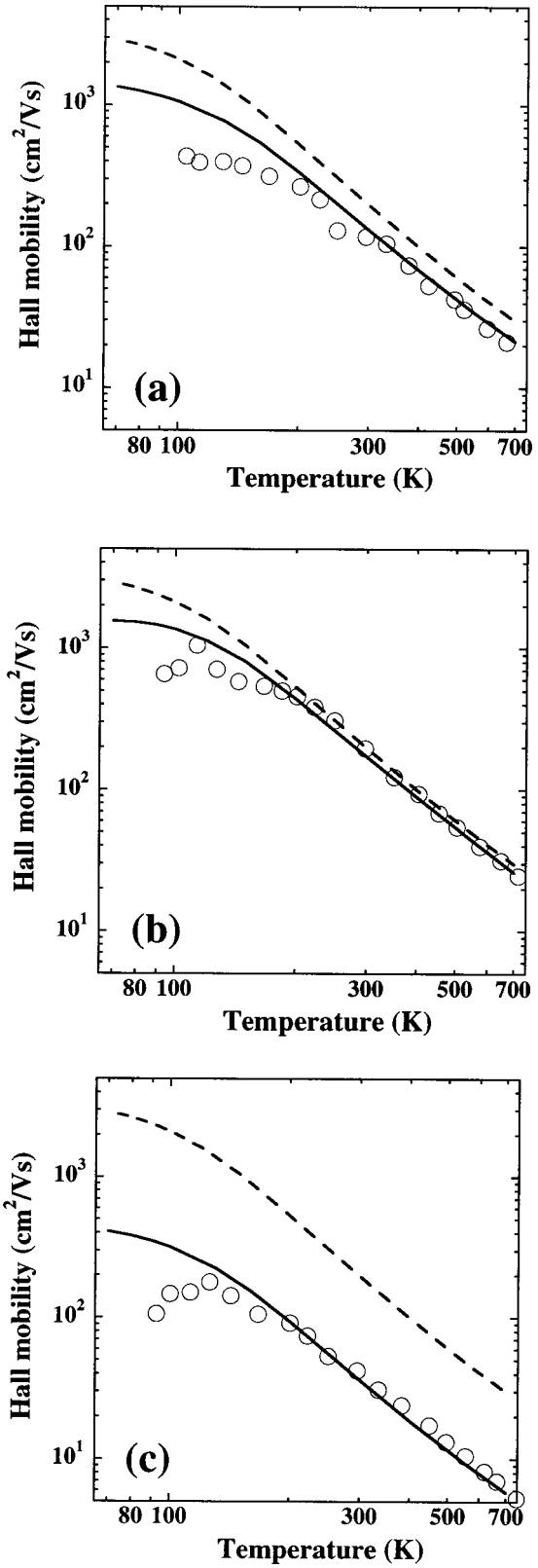

FIG. 4. Direct comparison of the Hall mobility as a function of temperature between the calculation based on the model developed in this work (solid curve), calculation assuming an isotropic band (dashed curve), and the experiment (open circles) for (a) [$\mathbf{j}\perp\mathbf{c},\mathbf{B}\|\mathbf{c}$], (b) [$\mathbf{j}\perp\mathbf{c},\mathbf{B}\perp\mathbf{c}$], and (c) [$\mathbf{j}\|\mathbf{c},\mathbf{B}\perp\mathbf{c}$] Hall measurement configurations.

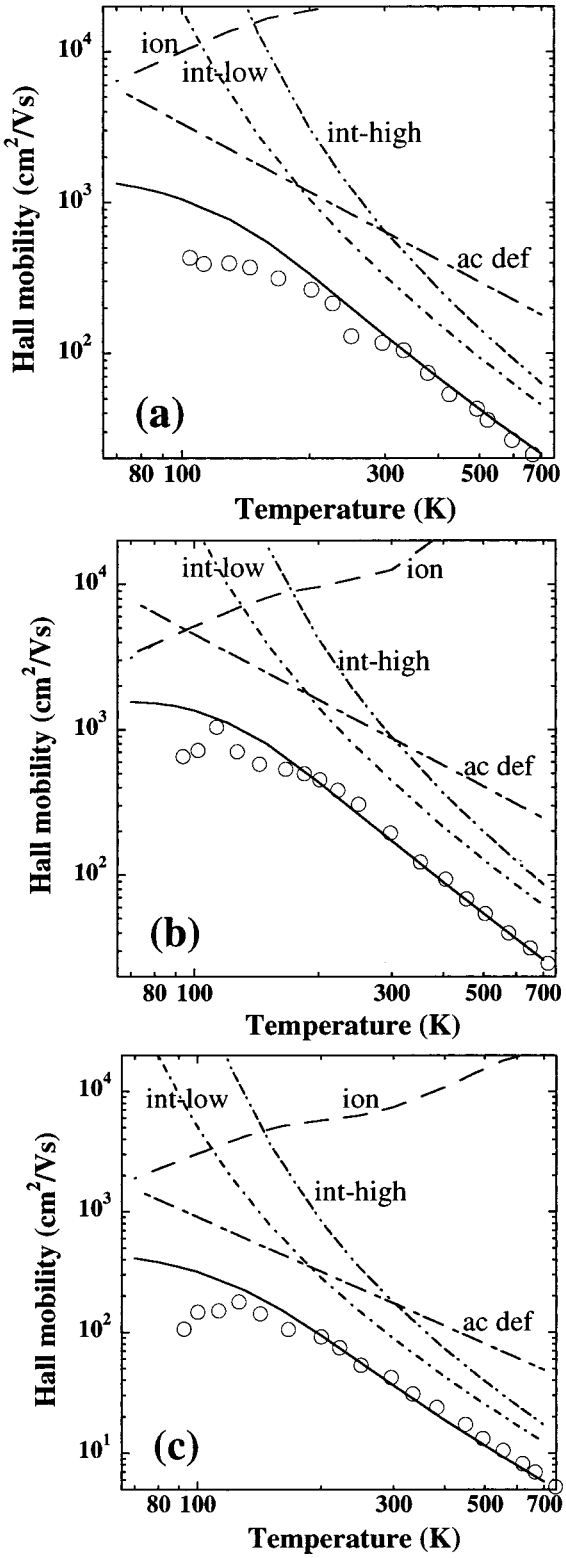

FIG. 5. Contribution of various scattering mechanisms to the total electron Hall mobility (solid curve) for (a) [$\mathbf{j}\perp\mathbf{c},\mathbf{B}\|\mathbf{c},$] (b) [$\mathbf{j}\perp\mathbf{c},\mathbf{B}\perp\mathbf{c},$] and (c) [$\mathbf{j}\|\mathbf{c},\mathbf{B}\perp\mathbf{c}$] measurement configurations. Scattering mechanisms shown are ionized impurity scattering (ion), acoustic phonon deformation scattering (ac def), intervalley scattering of high (int-high), and low (int-low) energy phonons.

ing a primitive version of our present model.[19] They are $\rho = 3.166\,\mathrm{g/cm^3}$, $v_s = 13.3\times10^5\,\mathrm{cm/s}$, $D_{ac} = 15\,\mathrm{eV}$, $\Theta_2 = 540\,\mathrm{K}$, $w_2/w_1 = 3$, $\Theta_3 = 870\,\mathrm{K}$, $w_3/w_1 = 3$, $\Theta_{\mathrm{op}} = 1066\,\mathrm{K}$, and $D_{\mathrm{op}} = 20\,\mathrm{eV}$. Consequently, our calculation does not contain any adjustable parameters, i.e., a direct comparison with experiments becomes possible.

Figures 4(a)–4(c) show the comparison of our Hall mobility calculation (solid curve) with experimentally measured

Hall mobilities (open circles) in the three configurations [$\mathbf{j}\perp\mathbf{c},\mathbf{B}\parallel\mathbf{c}$], [$\mathbf{j}\perp\mathbf{c},\mathbf{B}\perp\mathbf{c}$], and [$\mathbf{j}\parallel\mathbf{c},\mathbf{B}\perp\mathbf{c}$], respectively. Dashed curves are obtained from the same calculation using the isotropic density-of-states effective mass. The existence of the large Hall mobility anisotropy is evident from Figs. 4(a)–4(c). It is clearly shown that the model developed in this work agrees very well with experiments in all the three Hall effect configurations. The small deviation between calculation and experiment below 200 K is most likely due to the effect of hopping conduction. The hopping conduction at low temperatures tends to lower the mobility in the sample while our calculation neglects such an effect. The present calculation shows much better agreement with experiments than our previous work[19] since the effect of anisotropy on ionized impurity scattering is included. The result of the calculation using isotropic density-of-states effective mass does not agree at all with experiments as expected.

Figures 5(a)–5(c) show the contribution of the four scattering mechanisms to the total mobility. The scattering mechanisms shown in Fig. 5 are ionized impurity scattering (ion), acoustic phonon deformation scattering (ac def), intervalley scattering of high (int-high), and low (int-low) energy phonons. The effect of first-order optical phonon scattering is so small that it does not affect the curves show in Fig. 4. As is clear from Fig. 4, intervalley scattering dominates the mobility at high temperatures while acoustic phonon deformation scattering becomes important at low temperatures.

IV. CONCLUSION

We have developed a theoretical model describing drift and Hall mobilities of electrons in 6H–SiC. Analytical expressions for the drift and Hall mobility anisotropy have been obtained and used to calculate the Hall mobility for the three distinct Hall measurement configurations. The experimentally determined Hall mobility in *n*-type 6H–SiC agrees very well with the calculation based on our model.

ACKNOWLEDGMENTS

The authors thank Kyozaburo Takeda of Waseda University for fruitful discussions. Many useful comments by Hisaomi Iwata and Junichiro Muto are greatly appreciated.

[1] See, for example, a series of papers published in Phys. Status Solidi A **162** (1997).
[2] See, for example, a series of papers published in Phys. Status Solidi B **202** (1997).
[3] M. Schadt, G. Pensl, R. P. Devaty, W. J. Choyke, R. Stein, and D. Stephani, Appl. Phys. Lett. **65**, 312 (1994).
[4] W. J. Schaffer, G. H. Negley, K. G. Irvine, and J. W. Palmour, Mater. Res. Soc. Symp. Proc. **337**, 595 (1994).
[5] R. P. Joshi, J. Appl. Phys. **78**, 5518 (1995).
[6] R. P. Joshi and D. K. Ferry, Solid-State Electron. **38**, 1911 (1995).
[7] H.-E. Nilsson, U. Sannemo, and C. S. Petersson, J. Appl. Phys. **80**, 3365 (1996).
[8] R. Mickevicius and J. H. Zhao, J. Appl. Phys. **83**, 3161 (1998).
[9] The Hall mobility calculation for isotropic 3C–SiC has been performed theoretically by K. Tsukioka in *Silicon Carbide and Related Materials 1995*, Inst. Phys. Conf. Ser. No. 142, edited by S. Nakashima, H. Matsunami, S. Yoshida, and H. Harima (Institute of Physics, Bristol, 1996), p. 397.
[10] C. Persson and U. Lindefelt, Phys. Rev. B **54**, 10257 (1996).
[11] W. R. L. Lambrecht and B. Segall, Phys. Rev. B **52**, R2249 (1995).
[12] N. T. Son, O. Kordina, A. O. Konstantinov, W. M. Chen, E. Sörman, B. Monemar, and E. Janzén, Appl. Phys. Lett. **65**, 3209 (1994).
[13] M. Lundstrom, in *Fundamentals of Carrier Transport*, Modular Series on Solid State Devices, Vol. X (Addison-Wesley, Reading, MA, 1990), pp. 143–144.
[14] M. Lundstrom, in *Fundamentals of Carrier Transport*, Modular Series on Solid State Devices, Vol. X (Addison-Wesley, Reading, MA, 1990), p. 146.
[15] H. Brooks, Adv. Electron. Electron Phys. **7**, 85 (1955).
[16] D. K. Ferry, Phys. Rev. B **14**, 1605 (1976).
[17] W. Shockley, in *Electrons and Holes in Semiconductors* (Van Nostrand-Reinhold, Princeton, 1950).
[18] C. Herring, Bell Syst. Tech. J. **34**, 237 (1965).
[19] T. Kinoshita, K. M. Itoh, J. Muto, M. Schadt, G. Pensl, and K. Takeda, in *Silicion Carbide, III-Nitrides and Related Materials*, edited by G. Pensl, H. Morkoç, B. Monemar, and E. Janzén (Trans Tech, Switzerland, 1998), p. 295.